Using Importance Sampling Monte Carlo to Analyze Aircraft Takeoff and Landing

Jeffrey Ouellette*
NASA Langley Research Center, Hampton, Virginia, 23681, U.S.A.

Aircraft have achieved high levels of reliability, so the probability of undesirable dynamics is very low. The low probability of a bad takeoff or landing challenges nondeterministic methods to quantify the uncertainty of these improbable events. In the present work, a Monte Carlo method is defined to more effectively quantify these unlikely events that is suitable for uncertainty analysis of a mature design with many uncertainty parameters. The proposed Monte Carlo method has been applied to the takeoff and landing of the X-59 Quiet SuperSonic Technology (QueSST). Takeoff and landing simulation profiles were defined using a combination of industry standards and piloted simulation experience. The proposed method is shown to be able to quantify events with significantly fewer samples than would be required with conventional Monte Carlo. These results improve understanding of the sensitivity of the takeoff and landing dynamics to inform further studies and test planning.

I. Introduction

With any new aircraft there is significant uncertainty in the dynamics and performance characteristics. There is inherent variability in some maneuvers like takeoff and landing, such as the airspeed at which the aircraft touches down or the pilot executes the rotation. The significant variability of takeoff and landing compounds the uncertainty due to the limited knowledge of the system dynamics. It is desirable to achieve a better understanding of these uncertainties and to understand their effect on the operations of the aircraft before the beginning of the flight test campaign.

Fig. 1 The X-59 QueSST Aircraft (credit: NASA/Steve Freeman).

Monte Carlo methods are a typical approach to quantifying uncertainty and have been used for numerous aerospace vehicles [1–3]. A mature aircraft design can have hundreds of uncertain parameters, which causes a significant computational burden for many nondeterministic methods such as mu analysis [4–6]. Monte Carlo methods are appealing because the error converges independent to the number of uncertain parameters [7]. However, aircraft are generally very reliable systems with the probability of undesirable events being very low, on the order of 10^{-5} to 10^{-9} [8, 9]. In general, the number of required samples is inversely proportional to the probability, P_{occur}, such that it takes on the order of $\sim \frac{10}{P_{occur}}$ samples to get a good estimate of the probability. For all but the simplest computational models, this quickly becomes infeasible.

*Research Aerospace Engineer, Aeroelasticity Branch, Member AIAA.

By assuming a probability distribution for the quantity of interest, parametric methods have the potential to give better convergence [2]. Shakarian [3] used a parametric method to study the dispersion of landing metrics for various touchdown configurations to demonstrate the airworthiness of an autoland system. However, the requirement of a correct probability distribution can be a significant limitation on the ability to apply parametric methods. The nonlinearities in an aircraft simulation means that the quantities of interest often deviate from a normal or other analytical distribution.

To improve the applicability of the Monte Carlo methods to aerospace problems, an importance sampling method has been developed to give better estimates of these improbable events. The importance sampling method [7, 10] has been used to examine the robustness of takeoff and landing conditions of the X-59 Quiet SuperSonic Technology (QueSST) aircraft shown in Fig. 1. The Monte Carlo results are also used to show how one can gain better insights into the sensitivities of the aircraft that can be used to inform further analysis of flight test planning.

First, Section II provides the general description of the Monte Carlo importance sampling method and the related statistical definitions. Section III defines the simulation profiles used in the analysis of the takeoff and landing. In Section IV the method is applied to the X-59 QueSST.

II. Monte Carlo Methods

The simulations being used for the takeoff and landing are mature high-fidelity simulations. As a result, there are hundreds of parameters and corresponding uncertainties. To handle the high dimensionality of the simulation uncertainties, Monte Carlo methods are considered because their convergence is independent of the number of uncertainty parameters.

Monte Carlo convergence is independent of the number of parameters, but for events with a small probability, it can take a large number of samples to find a single case that shows the failure. For example, looking at Fig. 2a, we can see that only 2 samples have ended up in the region of interest.

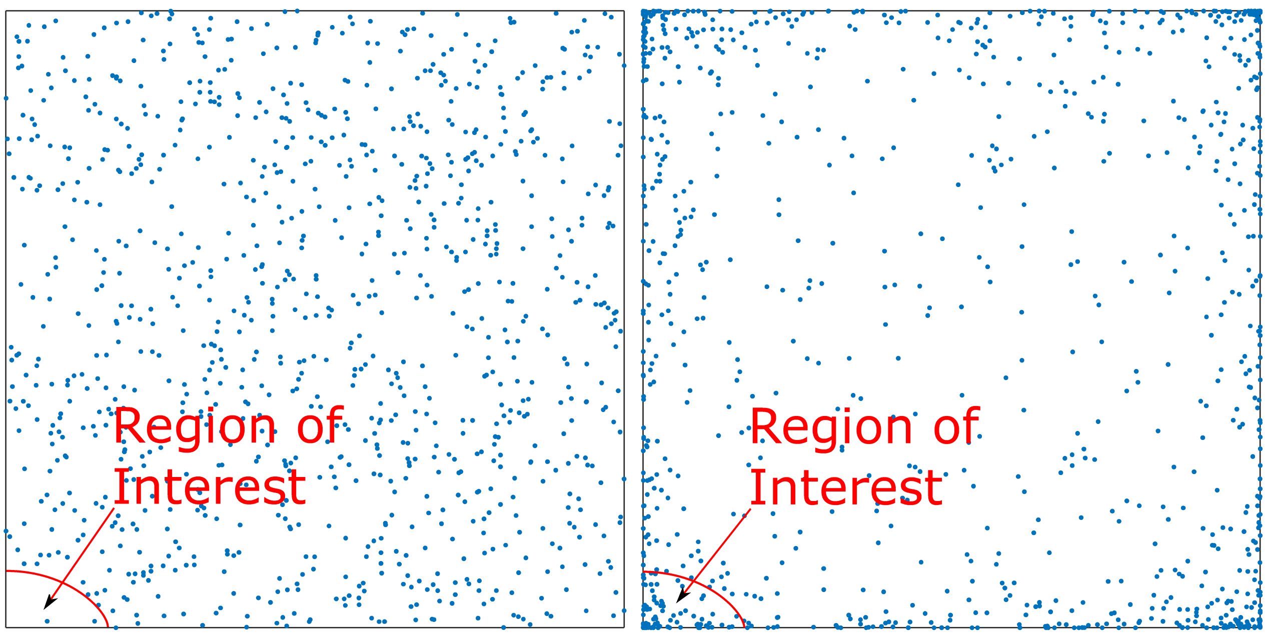

a) Example of Standard Monte Carlo Random Sampling.

b) Example of Importance Random Sampling.

Fig. 2 Random Sampling Methods.

However, if one were to change the sampling to focus on these regions of interest, as in Fig. 2b, we could get a much better estimate of the area. The approach demonstrated in Fig. 2b is called importance sampling [2, 7, 10], because we are sampling more from the region of interest which is the most important.

For the present analysis, the area of interest is the extremes of the parameters, so a sampling distribution with heaver tails is desired. To better characterize the tails of the output's probability distributions, a dispersion parameter, α, is defined along with the probability distributions in Section II.B. When $\alpha = 1$ the sampling matches the theoretical distribution exactly. As the dispersion parameter is decreased, $\alpha \to 0$, additional samples are taken from the extremes of the probability distributions. A correction is defined in Section II.A to adjust these results to give probabilities consistent with the defined probability distributions.

A. Importance Sampling

The most obvious approach to estimating the probability of an event, P_{fail}, is to take the ratio of the number of occurrences, n_{occur}, and the total number of samples, n_{sample}, as in Eq. (1).

$$P_{fail} = \frac{n_{occur}}{n_{sample}} \tag{1}$$

However, this becomes very challenging for events which have a low probability of occurring. Alternatively, the determination of the probability of occurrence can be expressed as an integration of the area of the parameter space, $\mathbf{x}$, in which there is an event over the total volume of the parameter space. The area where these events occur is called the region of interest, Eq. (2).

$$I(\mathbf{x}) = \begin{cases} 1 & \text{if occured} \\ 0 & \text{otherwise} \end{cases} \tag{2}$$

This concept has been illustrated for a 2-parameter case in Fig. (2). Even for cases of many more parameters, the total volume is very simple to determine. The challenge is that the boundary of the region of interest cannot be easily expressed or integrated. It is necessary to use some numerical method of integration. The large number of parameters make most numerical quadrature schemes impractical. However, the method of Monte Carlo integration Eq. (3) has an accuracy which is independent of the number of parameters. In Monte Carlo integration, the integral is replaced by a sum of random samples.

$$P_{fail} = \int \cdots \int I(\mathbf{x})\, d\mathbf{x} \approx \frac{1}{n_{sample}} \sum_{i}^{n_{sample}} I(\mathbf{x}_i) + O\left(\frac{1}{\sqrt{n_{samples}}}\right) \tag{3}$$

Applying the Monte Carlo integration directly gives the same result as Eq. (1). For a small region, it takes many samples to get a good estimate of that area. Initially, the idea of expressing the probability as an integral appears unhelpful. However, by expressing it as an integration allows the use of importance sampling.

In importance sampling, the approximation of the integral becomes a weighted sum, Eq. (4). The weighting, w, is a function of the probability density function (PDF) defined for the parameter, f, and the PDF used for sampling, $\tilde{f}$. Because each parameter is sampled independently, the probability of a sample is the product of the individual PDF. For numerical accuracy, the product is implemented using the summation of logarithms.

$$P_{fail} \approx \frac{1}{n_{sample}} \sum_{i}^{n_{sample}} \left(\prod_{j}^{n_{param}} w\left(x_{ij}\right) \right) I(\mathbf{x}_i) + O\left(\frac{1}{\sqrt{n_{samples}}}\right) \tag{4}$$

$$w\left(x_{ij}\right) \triangleq \frac{\tilde{f}\left(x_{ij}\right)}{f\left(x_{ij}\right)} \tag{5}$$

It is assumed that the extreme values of the parameters will be the most critical cases for the current margin sensitivity analysis. Because it is unclear which of the extreme values is the critical case, a symmetric distribution was used. The importance weights are the ratio of the PDFs in Eqs. (6a), (7a), and (8a) to the adjusted PDF in Eqs. (6b), (7b), and (8b).

Importance sampling is an effective method of examining the likelihood of events with a low probability. However, it does have some limitations and shortfalls. If the parameters are pushed too far to the extreme, then there will not be enough to effectively fill the region of interest. When these parameters are pushed too far, it can be seen in a very jagged visualization of the probability distribution or large jumps in estimate of the probability as more samples are added. The reason this occurs can be seen by looking at Fig. 2b. The importance sampling is putting many more points into the region of interest. However, there are fewer points close to the marginal edge of the region. If the points are pushed too far, the analysis can significantly under-predict the probability of events. However, it is still effective when looking at intervals and the range of the quantities of interest.

B. Probability Distributions

The values of the parameters for each simulation are drawn from three different probability distributions [11]: normal, uniform, and gamma. The basics of these distributions and the method for the importance sampling are defined here. For the present work, the probability distributions are defined by their mode (the most likely value), the variance, and a skew. Alternatively, a minimum and maximum value can be defined, and from these the variance and skew are calculated. The mode is selected as the nominal value used in the simulation.

The normal and gamma distributions allow arbitrarily large values, i.e., they have infinite supports. To avoid excessively large values which could break the simulation, a limit is applied to the parameters from these distributions. Based on the recommendations of MIL-A-8863C [12], the samples from normal and gamma distributions are truncated at a probability of 10^{-4}, which corresponds to approximately 3.7 standard deviations for a normal distribution.

1. Normal Distribution

The normal distribution, Eq. (6a), is one of the most common probability distributions. The normal distribution is symmetric about the mode and therefore the mode is equal to the mean, μ, or average. The dispersion of the normal distribution is defined by the variance, σ^2. The normal distribution has infinite supports, which means that it can be any value. The normal distribution is often the first choice in the distribution for a parameter. We only move to the other distributions when problems arise in using the normal distribution. The importance sampling for the normal distribution is accomplished by using a generalization of the normal distribution called a T-distribution, Eq. (6b). The T-distribution adds an additional parameter defined in Eq. (6c).

$$f_N(x) = \frac{1}{\sqrt{2\pi}} e^{-(x-\mu)^2/2\sigma^2} \tag{6a}$$

$$\tilde{f}_N(x;\alpha) = \frac{\Gamma\left(\frac{\nu+1}{2}\right)}{\sqrt{\pi\nu}\,\Gamma\left(\frac{\nu}{2}\right)} \left(1 + \frac{(x-\mu)^2}{\nu\sigma^2}\right)^{-\frac{\nu+1}{2}} \tag{6b}$$

$$\nu = 2 + \tanh^{-1}\alpha \tag{6c}$$

where $\Gamma()$ is the gamma function. When $\alpha = 1$ the T-distribution will be identical to a normal distribution.

2. Uniform Distribution

The second distribution is a uniform distribution. For the uniform distribution, all values are equally likely, but the values are limited in range. The uniform distribution is used for parameters where it is difficult to define a value which is most likely, e.g., fuel weight. The uniform distribution is also used for the aerodynamic parameters. The PDF for a uniform distribution is shown in Eq. (7a). A beta distribution, Eq. (7b), is used for the importance sampling.

$$f_U(x) = 1 \tag{7a}$$

$$\tilde{f}_U(x;\alpha) = \frac{x^{\alpha-1}(x-1)^{\alpha-1}}{B(\alpha,\alpha)} \tag{7b}$$

where $B(\alpha,\alpha)$ is the beta function.

The uniform distribution is a special case of the beta distribution so that when $\alpha = 1$ the beta distribution becomes the uniform distribution.

3. Gamma Distribution

The final distribution used is the Gamma distribution, Eq. (8a). The Gamma distribution is not symmetric, the mean is not equal to the mode. The gamma distribution is always positive, i.e., it has a support of $(0,\infty)$. The gamma distribution is used when there is a desired mode but there is also some lower bound required. For example, the sink rate must always be negative for landing. The MIL-A-8863C specifies a Pearson Type III (equivalent to the gamma distribution) for the sink rate at landing. The gamma distribution has also been used for the rotation speed during takeoff. The gamma distribution allows the rotation speed to be skewed so that the nominal is significantly lower than the maximum, but the minimum is still close to the nominal.

Unlike the other distributions, the Gamma distribution remains a gamma distribution when using the importance sampling, Eq. (8b). This was necessary to maintain the specified supports. For the importance sampling with the gamma distribution, the dispersion is increased by increasing the variance. The gamma distribution is defined by two parameters, a and b. To weigh the tails more heavily for importance sampling, these two parameters are modified in Eqs. (8c) and (8d). This parameterization ensures the mode and the supports remain unchanged.

$$
\begin{aligned}
f_\Gamma(x) &= \frac{1}{\Gamma(a+1)\, b^{a+1}} x^a e^{-x/b} && \text{(8a)}\\
\tilde{f}_\Gamma(x;\alpha) &= \frac{1}{\Gamma(\tilde{a}+1)\, \tilde{b}^{\tilde{a}+1}} x^{\tilde{a}} e^{-x/\tilde{b}} && \text{(8b)}\\
\tilde{a} &= (\alpha-1)\, a + 1 && \text{(8c)}\\
\tilde{b} &= \frac{b}{\alpha} && \text{(8d)}
\end{aligned}
$$

where $\Gamma()$ is the gamma function.

III. Simulation Profiles

Given the thousands of parameter combinations that were being examined, it is impractical to use a pilot to simulate each case. Instead, a set of inputs are defined that are similar to those used by the project pilots. The simulation used in the present analysis is a non-linear six-degree-of-freedom simulation developed and maintained by NASA Armstrong Flight Research Center [13–15]. The takeoff and landing profiles are both defined with respect to the landing reference speed, V_{ref}.

A. Takeoff Profile

Data and comments from two of the three project pilots was used to define these predefined inputs that could simulate the takeoff without a pilot in the cockpit. These simulations used to define the takeoff profile without a pilot were performed in the NASA Armstrong simulator. The two pilots use slightly different techniques, but there is enough common ground to find a reasonable and defensible approach to the predefined takeoff.

The current simulation profile uses a relatively abrupt pull on the stick. Based in part on the present analysis, a more gradual pull on the stick is favored, but the simulation profiles have not yet been updated to reflect the more gradual pull. Pilot A described his takeoff technique after the nose comes off of the ground as follows:

> "So, as you approach 8 degrees you start to reduce your aft stick to capture the pitch. Soon after your FPM [flight path marker] has settled and then you transition to setting a climb angle with the FPM."

The flight path marker is an indication in the cockpit of the flight path angle, γ, or the orientation of the aircraft's velocity vector relative to the earth. The data from a takeoff by Pilot A is shown in Fig. (3). The pilot stick is used to command vertical acceleration, ΔN_z. In Fig. (3), the actual stick fraction is scaled to match the ΔN_z command after the control law shaping. The stick is pulled back at 20 knots below V_{ref}, the nominal rotation speed. After the vehicle lifts off at $\sim$ 29 sec the pilot transitions to a desired γ.

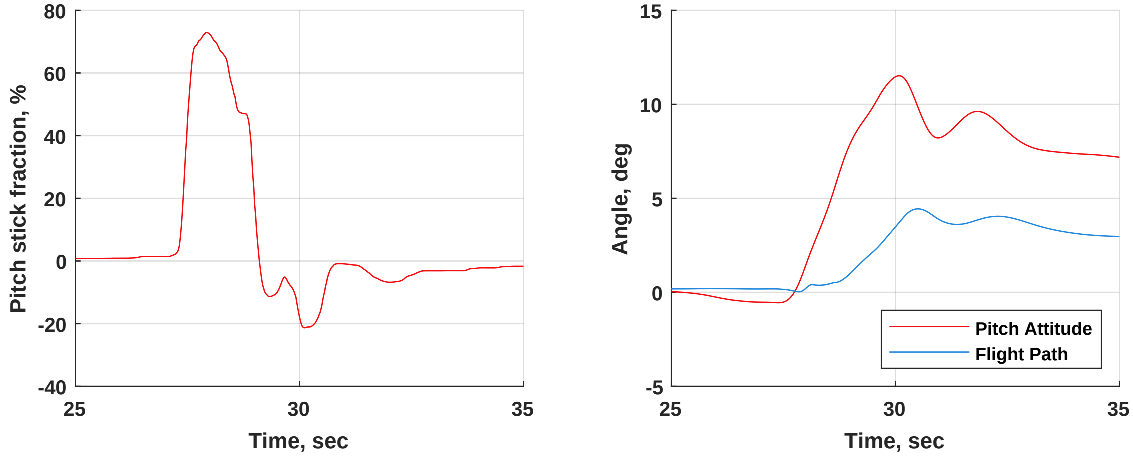

a) Pitch command during takeoff. **b) Pitch attitude and flight path angles during takeoff.**

Fig. 3 Pilot A takeoff technique.

A similar takeoff for Pilot B is shown in Fig. (4). You can see the pull at the nominal rotation speed.

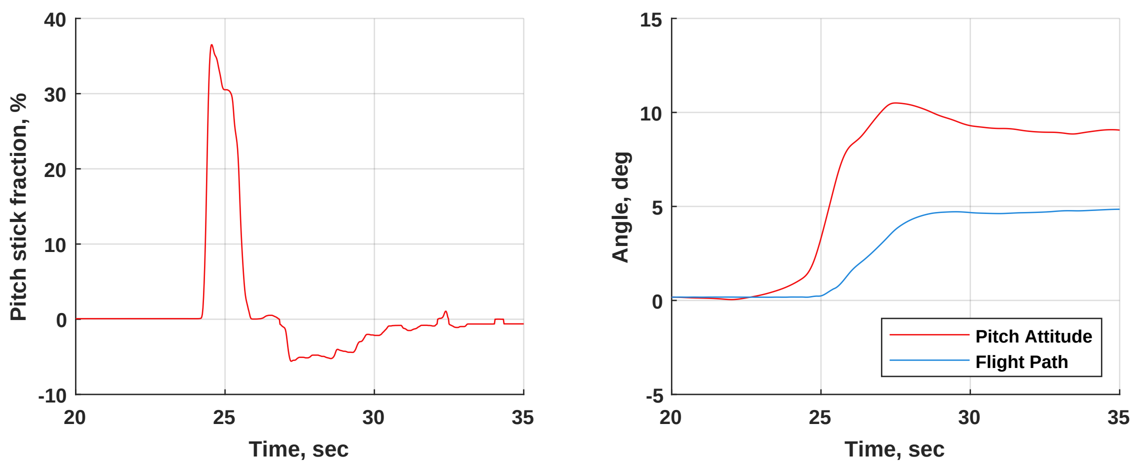

a) Pitch command during takeoff. **b) Pitch attitude and flight path angles during takeoff.**

Fig. 4 Pilot B takeoff technique.

The pilot described releasing after "getting away from the ground" which Figs. (3) and (4) show occurs after < 1 sec. From the data we can see the release appears to occur as soon as the rate of climb is positive. The positive rate of climb has been implemented as $\gamma > 0.5$ deg, to avoid attitude changes on the ground.

Unlike Pilot A, there is a release in the stick to the neutral position for several seconds between the pull and the γ tracking at ~ 27 sec. Pilot B indicated he did not want to push the stick forward close to the ground. It appears this technique produces a delay in the transition to arresting any pitch up motion and producing this period of neutral stick input. However, a criterion for this delay in transition could not be determined from the available data. As a result, this delay between the pull and the flight path angle tracking is not currently implemented.

Based on these piloted simulations, the takeoff is separated into three phases. Asterisks are used to indicate the parameters that were randomized in the Monte Carlo simulations.

- Apply military power
- At $V_{ref} - 20^*$ knots, pull to 50% stick over $\frac{1}{2}$ sec or until pitch attitude $> 7.5^*$ deg

- After $\gamma > 0.5$ deg, track $\gamma = 5^*$ deg

Previous analysis of the takeoff neglected the γ tracking, but this may be a problem when the pull alone is not sufficient to trim into a climb away from the ground for some uncertainty cases. The γ tracking is accomplished by a γ plus N_z feedback primarily to keep the aircraft moving away from the ground.

B. Landing Profile

The method of simulating landing is taken from MIL-A-8863C [12]. The aircraft is trimmed at 0.1 inches off the ground and at a gamma of roughly -0.5 deg. Initializing just above the ground allows better control over the touchdown attitude and replication of the variations due to pilot technique and turbulence. The initial conditions suggested by MIL-A-8863C are shown in Table (1). These were used as a starting point but were updated to be consistent with the X-59 flight manual and operating limits.

Table 1 Landing Impact Conditions from MIL-A-8863C for Land Based Aircraft. [12]

Description	Variable	Units		Value
Engaging ground speed	V_{TD}	knots	Mean	$1.05V_{ref}$
			Standard deviation	8.0
Sinking speed		knots	Mean	3.6
			Standard deviation	1.33
Pitch angle	θ	deg	Mean	Trim
			Standard deviation	2.25
Roll angle	ϕ	deg	Mean	0.0 and 2.0
			Standard deviation	2.5
Roll rate	p	dps	Mean	0.0
			Standard deviation	3.0

The mean and standard deviation of the sinking speed was updated to match the limits specified by the X-59 structural design criteria. Also, the engaging speed, the ground speed at touchdown, was updated to a fixed $V_{ref} + 8$ knots, which approximates the 5% specified in MIL-A-8863C. The standard deviation of the engaging speed was reduced by half to better match the variations in speeds that has been observed in piloted simulation. The pilot is likely to track V_{ref} more closely on the approach, but a higher variation in the engaging speed is expected due to variation in the flare. Based on these updates, the aircraft is trimmed at the following conditions,

- Sink rate of 2 ft/s. (1 to 6)
- Airspeed of $V_{ref} + 8$ knots (-7 to 23)
- Speed hold active
- Throttle at idle
- Bank angle 0 deg (-4.6 to 4.6)
- Roll rate 0 dps (-5.5 to 5.5)
- Altitude of 0.1 in

For each uncertainty case, if the flight manual values of V_{ref} result in an angle of attack greater than 6.5 deg, then V_{ref} is updated such that the aircraft will trim at 6.5 deg out of ground effect. Failing to adjust the V_{ref} results in cases that are on the alpha limiter and create operationally unrealistic responses. MIL-A-8863C specifies a pitch rate based on the touchdown speed in knots, V_{TD}, and load factor, N_z, as shown in Eq (9). The load factor was selected to be a fixed $N_z = 0.9$. This gave a pitch rate close to the observed values in simulations.

$$q = \dot{\alpha} \quad = \quad \frac{g}{1.69V_{TD}} \frac{180}{\pi} (N_z - 1) \text{ dps} \tag{9}$$

The speed hold disengages automatically on weight on wheels. The variations in the airspeed, bank angle, and roll rate are taken from MIL-A-8863C. These represent the variations due to noise, turbulence, or pilot technique.

IV. Results

The simulations were run with 2,000 combinations of the 131 (takeoff) or 130 (landing) parameters. With any Monte Carlo method, more samples is better, but 2,000 was a reasonable compromise between the computation time and convergence of results. The median importance sampling weight was found to be a reasonable rule of thumb for selecting the distribution parameter, α, for the importance sampling. In Eq. (10) the distribution parameter, α, was selected so that the median importance sampling weight was roughly 5×10^{-5}.

$$\alpha = 0.7 \tag{10}$$

For standard Monte Carlo, rather then the current importance sampling, these weights are a constant for all samples, Eq. 11.

$$\frac{1}{n_{sample}} = 5 \times 10^{-4} \tag{11}$$

The standard Monte Carlo is effective for probabilities about three times the weight in Eq. 11. If the parameter combinations have a probability of 5×10^{-4} of causing an output, such as angle of attack, to exceed a limit, then a standard Monte Carlo analysis has a 50% chance of actually finding that combination of parameters. If the probability of the parameter combinations causing the exceedance is 1.5×10^{-3}, then the standard Monte Carlo analysis would demonstrate the exceedance 95% of the time. These probability calculations do not exist for importance sampling, but a reasonable heuristic was found by looking at the box plot of the importance sampling weights in Fig. 5.

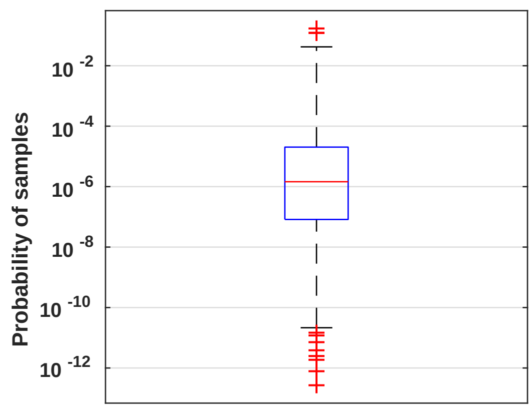

Fig. 5 Box Plot of Probability of Samples From Importance Sampling.

The blue box marks the interquartile range, where 75% of the data lies, and the red line marks the median, or middle of the data. The whiskers are used to identify which data points are outliers. These whiskers mark 1.5 times the interquartile range in each direction. The outliers are marked separately. The blue box in Fig. 5 shows that 75% the samples have probabilities between 10^{-5} and 10^{-7}. Therefore, the importance sampling is much more likely to give an accurate estimate of probabilities around 10^{-6}. The cost is that there are fewer samples close to the nominal and therefore events with probabilities around 10^{-2} will give poorer estimates then from standard Monte Carlo.

The same dispersion parameter was used for all parameters regardless of the probability distribution. Examples of each of the probability distributions are shown in Fig. 6. The raw PDF shows the distribution of the actual samples used in the simulation runs. The raw data is plotted partially transparent so that the corrected results can be seen behind it. The corrected results show the probability distribution after they are corrected with the importance sampling weights. This reflects the actual probability distribution defined for the parameter in the uncertainty model. The importance sampling is causing more samples at the extremes and fewer samples close to the nominal value.

The raw PDF of the uniformly distributed parameter in Fig. 6a shows a large increase in the number of samples at the extreme. The normal distribution, Fig. 6b, and Gamma distribution, Fig. 6c, do show an increase in the number of samples in the tail of the distribution. The increase in the number of samples in the normal and Gamma distribution is not as apparent as the uniform. However, because the probability in these tails are much lower the importance sampling is still significantly increasing the probability of a sample being drawn from these tails. The Gamma distribution, Fig. 6c, is one sided so the importance sampling is focused more in the higher range of values.

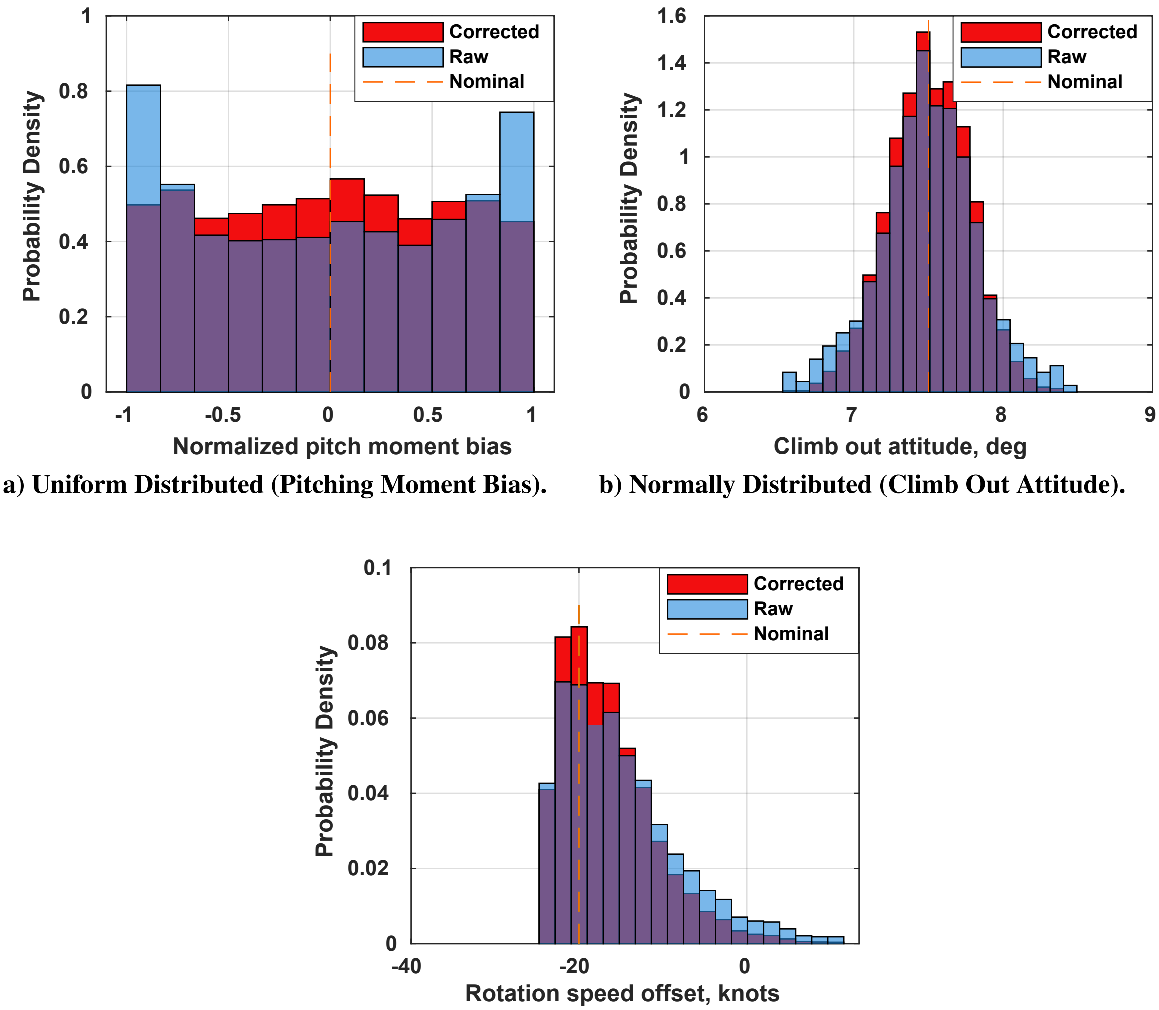

a) Uniform Distributed (Pitching Moment Bias).

b) Normally Distributed (Climb Out Attitude).

c) Gamma Distributed (Rotation Speed Offset).

Fig. 6 Examples of the Effect of the Dispersion Parameter On Each Probability Distribution.

A. Takeoff

The most obvious concern in takeoff is an over rotation. To consider over rotation, first the angle of attack at takeoff is shown in Fig. 7. A simulation with the parameters set to a maximum nose up aerodynamic uncertainty is also shown because intuition would suggest that this nose up moment case would be most likely to cause an over rotation. Figure 7a shows the collection of all the different time histories. To clarify where the traces are most dense, the maximum probability intervals are shown in Fig. 7b. These intervals give a better idea of what a typical response would look like. The Monte Carlo results show a much higher variation in the angle of attack than is demonstrated by the single nose up uncertainty.

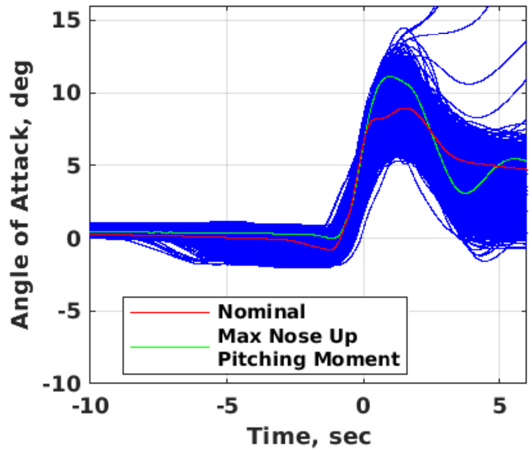

a) Plot of time traces.

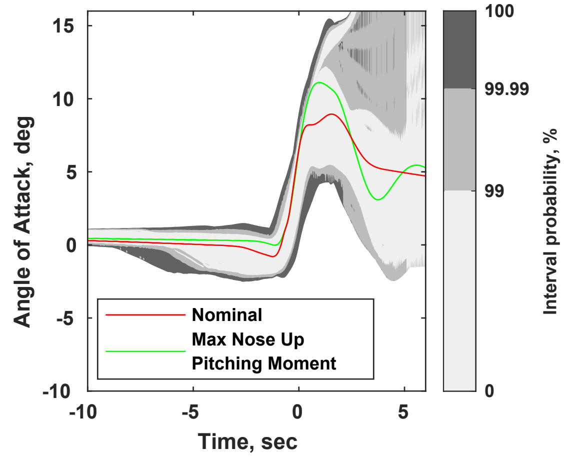

b) Plot of maximum probability intervals.

Fig. 7 Angle of Attack at Takeoff.

The probability distribution of the maximum angle of attack is shown in Fig. 8. The cumulative distribution is estimated by a histogram as well as kernel density estimate [16]. The kernel method generally gives a smoother density estimate that is easier to read and use, but the histogram gives a clearer picture of where the data is and how well the probability distribution has converged. The simulations are showing that without a pilot to recognize the fast rotation, there is a ~ 2% probability of exceeding 15 deg angle of attack during the rotation.

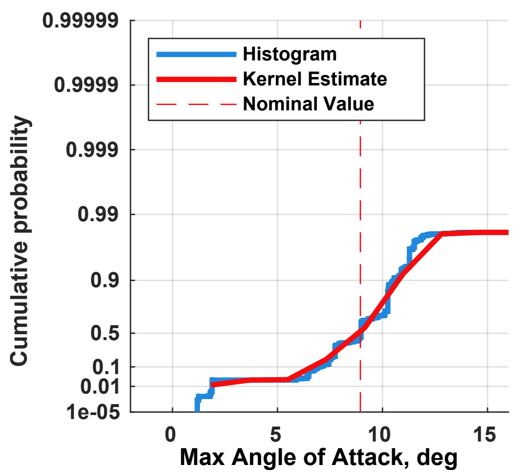

Fig. 8 Maximum Angle of Attack Probability at Takeoff.

Sobol indices were also used to assess the sensitivity of the angle of attack to each parameter. Sobol indices are the normalized contribution (a percentage) of each parameter to the total variations in the peak angle of attack simulated. A sparse polynomial chaos [17] was used to calculate the Sobol indices. The Wiener-Askey scheme of polynomials [18], which are orthogonal when weighted by the probability distributions, are used to generate a surrogate model of the angle of attack as a function of the uncertain parameters. The least absolute shrinkage and selection operator (LASSO) [16] is used to select which coefficients are dominating the response and generate a sparse model of the contributions to angle of attack, that is more easily interpretable. One factor at a time analysis, where each parameter is varied individually, showed very similar conclusions, but the polynomial chaos does offer the ability to capture the interaction between parameters.

The Sobol indices show that the angle of attack error accounts for 95% of the total variation in the peak angle of attack. The high sensitivity of the angle of attack sensor is because the X-59 control law uses a limiter to limit the angle of attack. The limiter generally prevents larger angles of attack on rotation, but if the sensor is underestimating by 3 deg, it will not arrest angle of attack until 3 deg later.

The N_z also shows overshoots in Fig. 9. The N_z shows a $\sim 2\%$ probability of exceeding 3 g.

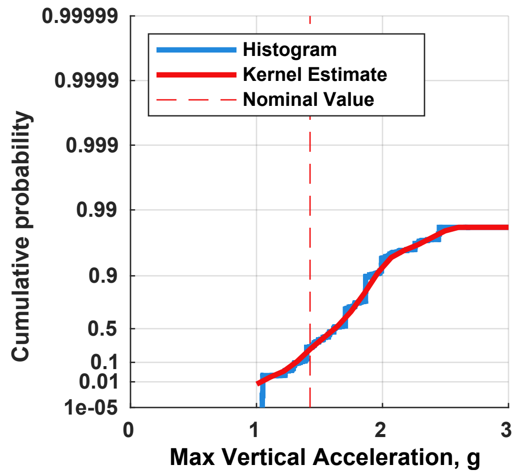

Fig. 9 Maximum Vertical Acceleration Probability at Takeoff.

The information from these simulations can be used to assess the effectiveness of changing the pilot technique or the conditions for takeoff to reduce the acceleration and loads or to avoid overshooting angle of attack. Because the engineers have a better idea of the parameters driving these uncertainties, ground testing can be planned to minimize potential errors in the angle of attack.

B. Landing

The angle of attack time history data from the landing Monte Carlo simulations are shown in Fig. 10. There are three cases in Fig. 10a that show a balloon like behavior and the aircraft is returning to flight. The balloon occurs when landing at a high speed with a significant nose up pitching moment. The probability intervals in Fig. 10b indicate that the probability is $< 10^{-4}$, the resolution of the probability intervals does not allow a more accurate estimate of the probability.

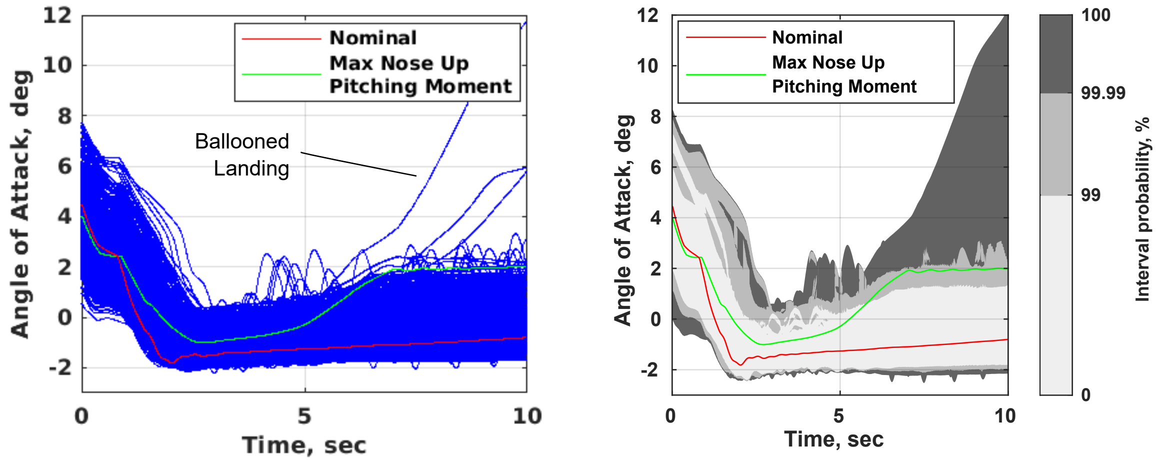

a) Plot of time traces.

b) Plot of maximum probability intervals.

Fig. 10 Angle of Attack at Landing.

To get a more accurate estimate of the probability, the cumulative distribution is shown in Fig. 11. The cumulative distribution is also limited because it is not distinguishing between the angle of attack at touchdown. However, if the maximum angle of attack exceeds 8 deg, it is typically due to the aircraft ballooning on landing. The analysis shows a probability $\sim 10^{-5}$ of the aircraft lifting off after landing. With only three cases showing the balloon, the probability is likely not accurate and additional tuning of the dispersion parameter, α, would be needed to get a better estimate. Traditional Monte Carlo would have required hundred of thousands of runs to identify this critical case, which is not feasible. In contrast, importance sampling allows identification of these critical cases with a fraction of the number of runs.

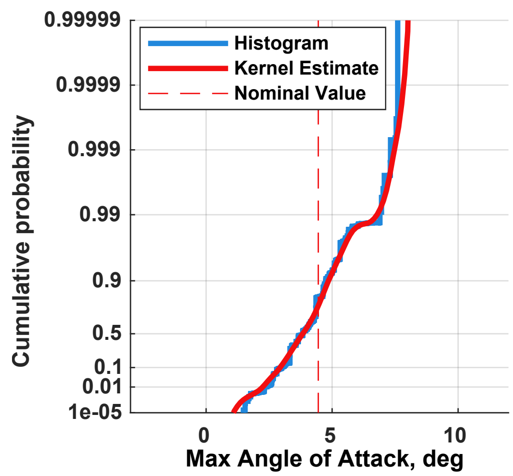

Fig. 11 Probability of Maximum Angle of Attack at Landing.

With better knowledge of what could cause a ballooned landing can aid the control room to monitor for these in flight and avoid landing fast if the aircraft is showing a higher-than-expected nose up moment, or to implement other mitigations.

V. Conclusion

A refinement of the Monte Carlo method has been developed that allows simulation and quantification of probabilities with significantly fewer simulation runs than would typically be required. The method was applied to analysis of the takeoff and landing of the X-59 QueSST. The analysis showed that the method was able to give a reasonable estimate of probabilities with $\frac{1}{2}$ to $\frac{1}{10}$ of the runs that would have been required for standard Monte Carlo. The methods were also effective on a problem with over 100 uncertain parameters and significant nonlinearities. Better quantification of these uncertainties was shown to be able to provide valuable insights to the engineers that can be used to improve the test efficiency.

Acknowledgments

This work has been supported by the NASA Low Boom Flight Demonstrator Project. The author acknowledges the contributions of the X-59 team at NASA Armstrong Flight Research Center, NASA Langley Research Center and Lockheed Martin Aeronautics. Additional technical conversations with Dave Cox and Nicholas Vazquez are acknowledged and appreciated.

References

[1] Baumann, E., Bahm, C., Strovers, B., Beck, R., and Richard, M., "The X-43A Six Degree of Freedom Monte Carlo Analysis," AIAA 2008-203, Reno, NV, 2008.
https://doi.org/10.2514/6.2008-203.

[2] Hanson, J. M., and Beard, B. B., "Applying Monte Carlo Simulation to Launch Vehicle Design and Requirements Analysis," NASA TP–2010–216447, Sep. 2010.

[3] Shakarian, A., "Application of Monte-Carlo techniques to the 757/767 autoland dispersion analysis by simulation," AIAA 1983–2193, Gatlinburg, TN, Aug. 1983.
https://doi.org/10.2514/6.1983-2193.

[4] Morton, B. G., and McAfoos, R. M., "A mu-test for robustness analysis of a real-parameter variation problem," Ieee, 1985.
https://doi.org/10.23919/ACC.1985.4788593.

[5] Poljak, S., and Rohn, J., "Checking robust nonsingularity is NP-hard," *Mathematics of Control, Signals and Systems*, Vol. 6, 1993, pp. 1–9.

[6] Lavretsky, E., and Wise, K. A., *Robust and Adaptive Control with Aerospace Applications*, Springer-Verlag London, 2024.

[7] Liu, J. S., *Monte Carlo Strategies in Scientific Computing*, Springer-Verlag, 2001.

[8] "System Design and Anaylsis," FAA AC 25.1306-1A, Jul. 1988.

[9] "Airworthiness Certification Criteria," MIL-HDBK-516C, Dec. 2014.

[10] Tokdar, S. T., and Kass, R. E., "Importance sampling: a review," *Wiley Online Library*, Vol. 2, No. 1, 2010.

[11] Beyer, W. H. (ed.), *CRC Standard Mathematical Tables*, CRC Press, Inc., FL, 1978.

[12] "Airplane Strength and Rigidity Ground Loads for Navy Acquired Airplanes," MIL-A-8863C, Jul. 1993.

[13] Norlin, K. A., "Flight Simulation Software at NASA Dryden Flight Research Center," NASA TM–104315, Oct. 1995.

[14] Clarke, R., Lintereur, L., and Bahm, C., "Documenting the NASA Armstrong Flight Research Center Oblate Earth Simulation Equations of Motion and Integration Algorithm," NASA TP-–2016-–218956, Jan. 2016.

[15] Curlett, B. P., "A Software Framework for Aircraft Simulation," NASA TP-–2008-–214639, Oct. 2008.

[16] Hastie, T., Tibshirani, R., and Friedman, J., *The Elements of Statistical Learning: Data Mining, Inference, and Prediction*, Springer series in statistics, Springer, 2009.

[17] Lüthen, N., Marelli, S., and Sudret, B., "Sparse polynomial chaos expansions: Literature survey and benchmark," *SIAM/ASA Journal on Uncertainty Quantification*, Vol. 9, No. 2, 2021, pp. 593–649.
https://doi.org/10.1137/20M1315774.

[18] Xiu, D., and Karniadakis, G. E., "The Wiener–Askey polynomial chaos for stochastic differential equations," *SIAM journal on scientific computing*, Vol. 24, No. 2, 2002, pp. 619–644.
https://doi.org/10.1137/S1064827501387826.